
Multi-source Domain Adaptation for Semantic Segmentation

Sicheng Zhao^{1*}†, Bo Li^{23†}, Xiangyu Yue^{1†}, Yang Gu²,
Pengfei Xu², Runbo Hu², Hua Chai², Kurt Keutzer¹

¹University of California, Berkeley, USA ²Didi Chuxing, China

³Harbin Institute of Technology, China

schzhao@gmail.com, drluodian@gmail.com, {xyyue, keutzer}@berkeley.edu
{guyangdavid, xupengfeipf, hurunbo, chaihua}@didiglobal.com

Abstract

Simulation-to-real domain adaptation for semantic segmentation has been actively studied for various applications such as autonomous driving. Existing methods mainly focus on a single-source setting, which cannot easily handle a more practical scenario of multiple sources with different distributions. In this paper, we propose to investigate multi-source domain adaptation for semantic segmentation. Specifically, we design a novel framework, termed Multi-source Adversarial Domain Aggregation Network (MADAN), which can be trained in an end-to-end manner. First, we generate an adapted domain for each source with *dynamic semantic consistency* while aligning at the pixel-level cycle-consistently towards the target. Second, we propose *sub-domain aggregation discriminator* and *cross-domain cycle discriminator* to make different adapted domains more closely aggregated. Finally, feature-level alignment is performed between the aggregated domain and target domain while training the segmentation network. Extensive experiments from synthetic GTA and SYNTHIA to real Cityscapes and BDDS datasets demonstrate that the proposed MADAN model outperforms state-of-the-art approaches. Our source code is released at: <https://github.com/Luodian/MADAN>.

1 Introduction

Semantic segmentation assigns a semantic label (*e.g.* car, cyclist, pedestrian, road) to each pixel in an image. This computer vision kernel plays a crucial role in many applications, ranging from autonomous driving [1] and robotic control [2] to medical imaging [3] and fashion recommendation [4]. With the advent of deep learning, especially convolutional neural networks (CNNs), several end-to-end approaches have been proposed for semantic segmentation [5, 6, 7, 8, 9, 10, 11, 12, 13, 14]. Although these methods have achieved promising results, they suffer from some limitations. On the one hand, training these methods requires large-scale labeled data with pixel-level annotations, which is prohibitively expensive and time-consuming to obtain. For example, it takes about 90 minutes to label each image in the Cityscapes dataset [15]. On the other hand, they cannot well generalize their learned knowledge to new domains, because of the presence of *domain shift* or *dataset bias* [16, 17].

To sidestep the cost of data collection and annotation, unlimited amounts of synthetic labeled data can be created from simulators like CARLA and GTA-V [18, 19, 20], thanks to the progress in graphics and simulation infrastructure. To mitigate the gap between different domains, domain adaptation (DA) or knowledge transfer techniques have been proposed [21] with both theoretical analysis [22,

*Corresponding Author.

†Equal Contribution.

23, 24, 25] and algorithm design [26, 27, 28, 29, 30, 31, 32]. Besides the traditional task loss on the labeled source domain, deep unsupervised domain adaptation (UDA) methods are generally trained with another loss to deal with domain shift, such as a discrepancy loss [31, 33, 34, 35], adversarial loss [36, 37, 38, 39, 40, 41, 42, 43, 44], reconstruction loss [30, 45, 46], *etc.* Current simulation-to-real DA methods for semantic segmentation [47, 48, 49, 50, 51, 52, 53, 54, 55, 56] all focus on the single-source setting and do not consider a more practical scenario where the labeled data are collected from multiple sources with different distributions. Simply combining different sources into one source and directly employing single-source DA may not perform well, since images from different source domains may interfere with each other during the learning process [57].

Early efforts on multi-source DA (MDA) used shallow models [58, 59, 60, 61, 62, 63, 64, 65, 66, 67]. Recently, some multi-source deep UDA methods have been proposed which only focus on image classification [68, 69, 70]. Directly extending these MDA methods from classification to segmentation may not perform well due to the following reasons. (1) Segmentation is a structured prediction task, the decision function of which is more involved than classification because it has to resolve the predictions in an exponentially large label space [48, 71]. (2) Current MDA methods mainly focus on feature-level alignment, which only aligns high-level information. This may be enough for coarse-grained classification tasks, but it is obviously insufficient for fine-grained semantic segmentation, which performs pixel-wise prediction. (3) These MDA methods only align each source and target pair. Although different sources are matched towards the target, there may exist significant mis-alignment across different sources.

To address the above challenges, in this paper we propose a novel framework, termed Multi-source Adversarial Domain Aggregation Network (MADAN), which consists of Dynamic Adversarial Image Generation, Adversarial Domain Aggregation, and Feature-aligned Semantic Segmentation. First, for each source, we generate an adapted domain using a Generative Adversarial Network (GAN) [36] with cycle-consistency loss [39], which enforces pixel-level alignment between source images and target images. To preserve the semantics before and after image translation, we propose a novel semantic consistency loss by minimizing the KL divergence between the source predictions of a pretrained segmentation model and the adapted predictions of a *dynamic segmentation model*. Second, instead of training a classifier for each source domain [68, 70], we propose *sub-domain aggregation discriminator* to directly make different adapted domains indistinguishable, and *cross-domain cycle discriminator* to discriminate between the images from each source and the images transferred from other sources. In this way, different adapted domains can be better aggregated into a more unified domain. Finally, the segmentation model is trained based on the aggregated domain, while enforcing feature-level alignment between the aggregated domain and the target domain.

In summary, our contributions are three-fold. (1) We propose to perform domain adaptation for semantic segmentation from multiple sources. To the best of our knowledge, this is the first work on multi-source structured domain adaptation. (2) We design a novel framework termed MADAN to do MDA for semantic segmentation. Besides feature-level alignment, pixel-level alignment is further considered by generating an adapted domain for each source cycle-consistently with a novel dynamic semantic consistency loss. Sub-domain aggregation discriminator and cross-domain cycle discriminator are proposed to better align different adapted domains. (3) We conduct extensive experiments from synthetic GTA [18] and SYNTHIA [19] to real Cityscapes [15] and BDDS [72] datasets, and the results demonstrate the effectiveness of our proposed MADAN model.

2 Problem Setup

We consider the unsupervised MDA scenario, in which there are multiple labeled source domains S_1, S_2, \dots, S_M , where M is number of sources, and one unlabeled target domain T . In the i th source domain S_i , suppose $X_i = \{\mathbf{x}_i^j\}_{j=1}^{N_i}$ and $Y_i = \{\mathbf{y}_i^j\}_{j=1}^{N_i}$ are the observed data and corresponding labels drawn from the source distribution $p_i(\mathbf{x}, \mathbf{y})$, where N_i is the number of samples in S_i . In the target domain T , let $X_T = \{\mathbf{x}_T^j\}_{j=1}^{N_T}$ denote the target data drawn from the target distribution $p_T(\mathbf{x}, \mathbf{y})$ without label observation, where N_T is the number of target samples. Unless otherwise specified, we have two assumptions: (1) homogeneity, *i.e.* $\mathbf{x}_i^j \in \mathbb{R}^d, \mathbf{x}_T^j \in \mathbb{R}^d$, indicating that the data from different domains are observed in the same image space but with different distributions; (2) closed set, *i.e.* $\mathbf{y}_i^j \in \mathcal{Y}, \mathbf{y}_T^j \in \mathcal{Y}$, where \mathcal{Y} is the label set, which means that all the domains share the same space of classes. Based on covariate shift and concept drift [21], we aim to learn an

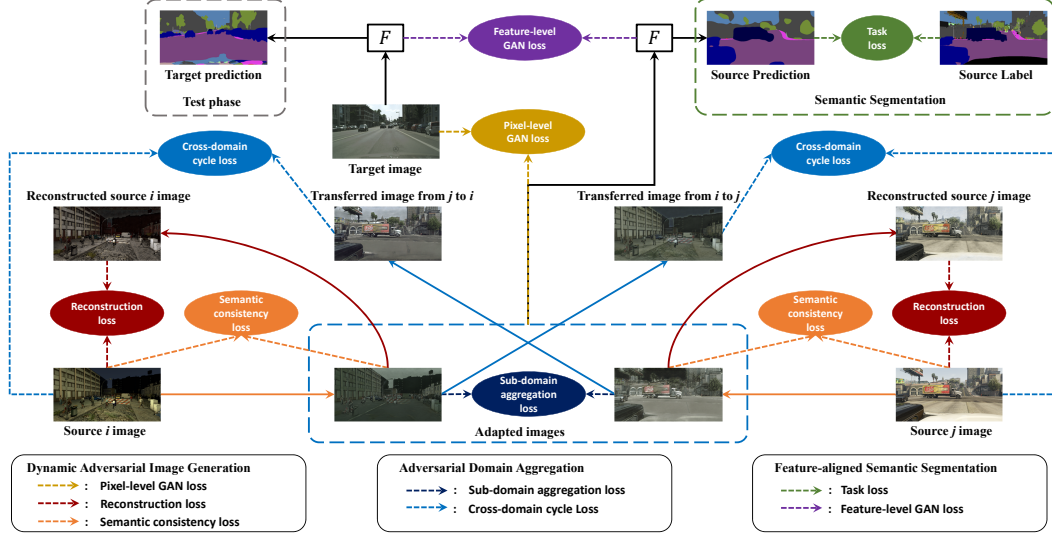


Figure 1: The framework of the proposed Multi-source Adversarial Domain Aggregation Network (MADAN). The colored solid arrows represent generators, while the black solid arrows indicate the segmentation network F . The dashed arrows correspond to different losses.

adaptation model that can correctly predict the labels of a sample from the target domain trained on $\{(X_i, Y_i)\}_{i=1}^M$ and $\{X_T\}$.

3 Multi-source Adversarial Domain Aggregation Network

In this section, we introduce the proposed Multi-source Adversarial Domain Aggregation Network (MADAN) for semantic segmentation adaptation. The framework is illustrated in Figure 1, which consists of three components: Dynamic Adversarial Image Generation (DAIG), Adversarial Domain Aggregation (ADA), and Feature-aligned Semantic Segmentation (FSS). DAIG aims to generate adapted images from source domains to the target domain from the perspective of visual appearance while preserving the semantic information with a dynamic segmentation model. In order to reduce the distances among the adapted domains and thus generate a more aggregated unified domain, ADA is proposed, including Cross-domain Cycle Discriminator (CCD) and Sub-domain Aggregation Discriminator (SAD). Finally, FSS learns the domain-invariant representations at the feature-level in an adversarial manner. Table 1 compares MADAN with several state-of-the-art DA methods.

3.1 Dynamic Adversarial Image Generation

The goal of DAIG is to make images from different source domains visually similar to the target images, as if they are drawn from the same target domain distribution. To this end, for each source domain S_i , we introduce a generator $G_{S_i \rightarrow T}$ mapping to the target T in order to generate adapted images that fool D_T , which is a pixel-level adversarial discriminator. D_T is trained simultaneously with each $G_{S_i \rightarrow T}$ to classify real target images X_T from adapted images $G_{S_i \rightarrow T}(X_i)$. The corresponding GAN loss function is:

$$\mathcal{L}_{GAN}^{S_i \rightarrow T}(G_{S_i \rightarrow T}, D_T, X_i, X_T) = \mathbb{E}_{\mathbf{x}_i \sim X_i} \log D_T(G_{S_i \rightarrow T}(\mathbf{x}_i)) + \mathbb{E}_{\mathbf{x}_T \sim X_T} \log[1 - D_T(\mathbf{x}_T)]. \quad (1)$$

Since the mapping $G_{S_i \rightarrow T}$ is highly under-constrained [36], we employ an inverse mapping $G_{T \rightarrow S_i}$ as well as a cycle-consistency loss [39] to enforce $G_{T \rightarrow S_i}(G_{S_i \rightarrow T}(\mathbf{x}_i)) \approx \mathbf{x}$ and vice versa. Similarly, we introduce D_i to classify X_i from $G_{T \rightarrow S_i}(X_T)$, with the following GAN loss:

$$\mathcal{L}_{GAN}^{T \rightarrow S_i}(G_{T \rightarrow S_i}, D_i, X_T, X_i) = \mathbb{E}_{\mathbf{x}_i \sim X_i} \log[1 - D_i(\mathbf{x}_i)] + \mathbb{E}_{\mathbf{x}_T \sim X_T} \log D_i(G_{T \rightarrow S_i}(\mathbf{x}_T)). \quad (2)$$

Table 1: Comparison of the proposed MADAN model with several state-of-the-art domain adaptation methods. The full names of each property from the second to the last columns are pixel-level alignment, feature-level alignment, semantic consistency, cycle consistency, multiple sources, domain aggregation, one task network, and fine-grained prediction, respectively.

	pixel	feat	sem	cycle	multi	aggr	one	fine
ADDA [25]	✗	✓	–	–	✗	–	✓	✓
CycleGAN [39]	✓	✗	✗	✓	✗	–	✓	✗
PiexlDA [37]	✓	✗	✗	✗	✗	–	✓	✓
SBADA [41]	✓	✗	✓	✓	✗	–	✓	✗
GTA-GAN [42]	✓	✓	✗	✗	✗	–	✓	✗
DupGAN [43]	✓	✓	✓	✗	✗	–	✓	✗
CyCADA [32]	✓	✓	✓	✓	✗	–	✓	✓
DCTN [68]	✗	✓	–	–	✓	✗	✗	✗
MDAN [69]	✗	✓	–	–	✓	✗	✓	✗
MMN [70]	✗	✓	–	–	✓	✗	✗	✗
MADAN (ours)	✓	✓	✓	✓	✓	✓	✓	✓

The cycle-consistency loss [39] ensures that the learned mappings $G_{S_i \rightarrow T}$ and $G_{T \rightarrow S_i}$ are cycle-consistent, thereby preventing them from contradicting each other, is defined as:

$$\mathcal{L}_{cyc}^{S_i \leftrightarrow T}(G_{S_i \rightarrow T}, G_{T \rightarrow S_i}, X_i, X_T) = \mathbb{E}_{\mathbf{x}_i \sim X_i} \|G_{T \rightarrow S_i}(G_{S_i \rightarrow T}(\mathbf{x}_i)) - \mathbf{x}_i\|_1 + \mathbb{E}_{\mathbf{x}_T \sim X_T} \|G_{S_i \rightarrow T}(G_{T \rightarrow S_i}(\mathbf{x}_T)) - \mathbf{x}_T\|_1. \quad (3)$$

The adapted images are expected to contain the same semantic information as original source images, but the semantic consistency is only partially constrained by the cycle consistency loss. The semantic consistency loss in CyCADA [32] was proposed to better preserve semantic information. \mathbf{x}_i and $G_{S_i \rightarrow T}(\mathbf{x}_i)$ are both fed into a segmentation model F_i pretrained on (X_i, Y_i) . However, since \mathbf{x}_i and $G_{S_i \rightarrow T}(\mathbf{x}_i)$ are from different domains, employing the same segmentation model, *i.e.* F_i , to obtain the segmentation results and then computing the semantic consistency loss may be detrimental to image generation. Ideally, the adapted images $G_{S_i \rightarrow T}(\mathbf{x}_i)$ should be fed into a network F_T trained on the target domain, which is infeasible since target domain labels are not available in UDA. Instead of employing F_i on $G_{S_i \rightarrow T}(\mathbf{x}_i)$, we propose to dynamically update the network F_A , which takes $G_{S_i \rightarrow T}(\mathbf{x}_i)$ as input, so that its optimal input domain (the domain that the network performs best on) gradually changes from that of F_i to F_T . We employ the task segmentation model F trained on the adapted domain as F_A , *i.e.* $F_A = F$, which has two advantages: (1) $G_{S_i \rightarrow T}(\mathbf{x}_i)$ becomes the optimal input domain of F_A , and as F is trained to have better performance on the target domain, the semantic loss after F_A would promote $G_{S_i \rightarrow T}$ to generate images that are closer to target domain at the pixel-level; (2) since F_A and F can share the parameters, no additional training or memory space is introduced, which is quite efficient. The proposed dynamic semantic consistency (DSC) loss is:

$$\mathcal{L}_{sem}^{S_i}(G_{S_i \rightarrow T}, X_i, F_i, F_A) = \mathbb{E}_{\mathbf{x}_i \sim X_i} KL(F_A(G_{S_i \rightarrow T}(\mathbf{x}_i)) || F_i(\mathbf{x}_i)), \quad (4)$$

where $KL(\cdot || \cdot)$ is the KL divergence between two distributions.

3.2 Adversarial Domain Aggregation

We can train different segmentation models for each adapted domain and combine different predictions with specific weights for target images [68, 70], or we can simply combine all adapted domains together and train one model [69]. In the first strategy, it is challenging to determine how to select the weights for different adapted domains. Moreover, each target image needs to be fed into all segmentation models at reference time, and this is rather inefficient. For the second strategy, since the alignment space is high-dimensional, although the adapted domains are relatively aligned with the target, they may be significantly mis-aligned with each other. In order to mitigate this issue, we propose adversarial domain aggregation to make different adapted domains more closely aggregated with two kinds of discriminators. One is the sub-domain aggregation discriminator (SAD), which is designed to directly make the different adapted domains indistinguishable. For S_i , a discriminator D_A^i is introduced with the following loss function:

$$\mathcal{L}_{SAD}^{S_i}(G_{S_1 \rightarrow T}, \dots, G_{S_i \rightarrow T}, \dots, G_{S_M \rightarrow T}, D_A^i) = \mathbb{E}_{\mathbf{x}_i \sim X_i} \log D_A^i(G_{S_i \rightarrow T}(\mathbf{x}_i)) + \frac{1}{M-1} \sum_{j \neq i} \mathbb{E}_{\mathbf{x}_j \sim X_j} \log[1 - D_A^i(G_{S_j \rightarrow T}(\mathbf{x}_j))]. \quad (5)$$

The other is the cross-domain cycle discriminator (CCD). For each source domain S_i , we transfer the images from the adapted domains $G_{S_j \rightarrow T}(X_j)$, $j = 1, \dots, M, j \neq i$ back to S_i using $G_{T \rightarrow S_i}$ and employ the discriminator D_i to classify X_i from $G_{T \rightarrow S_i}(G_{S_j \rightarrow T}(X_j))$, which corresponds to the following loss function:

$$\mathcal{L}_{CCD}^{S_i}(G_{T \rightarrow S_1}, \dots, G_{T \rightarrow S_{i-1}}, G_{T \rightarrow S_{i+1}}, \dots, G_{T \rightarrow S_M}, G_{S_i \rightarrow T}, D_i) = \mathbb{E}_{\mathbf{x}_i \sim X_i} \log D_i(\mathbf{x}_i) + \frac{1}{M-1} \sum_{j \neq i} \mathbb{E}_{\mathbf{x}_j \sim X_j} \log[1 - D_i(G_{T \rightarrow S_i}(G_{S_j \rightarrow T}(\mathbf{x}_j)))] \quad (6)$$

Please note that using a more sophisticated combination of different discriminators' losses to better aggregate the domains with larger distances might improve the performance. We leave this as future work and would explore this direction by dynamic weighting of the loss terms and incorporating some prior domain knowledge of the sources.

3.3 Feature-aligned Semantic Segmentation

After adversarial domain aggregation, the adapted images of different domains $X'_i (i = 1, \dots, M)$ are more closely aggregated and aligned. Meanwhile, the semantic consistency loss in dynamic adversarial image generation ensures that the semantic information, *i.e.* the segmentation labels, is preserved before and after image translation. Suppose the images of the unified aggregated domain are $X' = \bigcup_{i=1}^M X'_i$ and corresponding labels are $Y = \bigcup_{i=1}^M Y_i$. We can then train a task segmentation model F based on X' and Y with the following cross-entropy loss:

$$\mathcal{L}_{task}(F, X', Y) = -\mathbb{E}_{(\mathbf{x}', y) \sim (X', Y)} \sum_{l=1}^L \sum_{h=1}^H \sum_{w=1}^W \mathbb{1}_{[l=y_{h,w}]} \log(\sigma(F_{l,h,w}(\mathbf{x}'))), \quad (7)$$

where L is the number of classes, H, W are the height and width of the adapted images, σ is the softmax function, $\mathbb{1}$ is an indicator function, and $F_{l,h,w}(\mathbf{x}')$ is the value of $F(\mathbf{x}')$ at index (l, h, w) .

Further, we impose a feature-level alignment between X' and X_T , which can improve the segmentation performance during inference of X_T on the segmentation model F . We introduce a discriminator D_F to achieve this goal. The feature-level GAN loss is defined as:

$$\mathcal{L}_{feat}(F_f, D_{F_f}, X', X_T) = \mathbb{E}_{\mathbf{x}' \sim X'} \log D_{F_f}(F_f(\mathbf{x}')) + \mathbb{E}_{\mathbf{x}_T \sim X_T} \log[1 - D_{F_f}(F_f(\mathbf{x}_T))], \quad (8)$$

where $F_f(\cdot)$ is the output of the last convolution layer (*i.e.* a feature map) of the encoder in F .

3.4 MADAN Learning

The proposed MADAN learning framework utilizes adaptation techniques including pixel-level alignment, cycle-consistency, semantic consistency, domain aggregation, and feature-level alignment. Combining all these components, the overall objective loss function of MADAN is:

$$\begin{aligned} \mathcal{L}_{MADAN}(G_{S_1 \rightarrow T} \cdots G_{S_M \rightarrow T}, G_{T \rightarrow S_1} \cdots G_{T \rightarrow S_M}, D_1 \cdots D_M, D_A^1 \cdots D_A^M, D_{F_f}, F) \\ = \sum_i \left[\mathcal{L}_{GAN}^{S_i \rightarrow T}(G_{S_i \rightarrow T}, D_T, X_i, X_T) + \mathcal{L}_{GAN}^{T \rightarrow S_i}(G_{T \rightarrow S_i}, D_i, X_T, X_i) \right. \\ + \mathcal{L}_{cyc}^{S_i \leftrightarrow T}(G_{S_i \rightarrow T}, G_{T \rightarrow S_i}, X_i, X_T) + \mathcal{L}_{sem}^{S_i}(G_{S_i \rightarrow T}, X_i, F_i, F) \\ + \mathcal{L}_{SAD}^{S_i}(G_{S_1 \rightarrow T}, \dots, G_{S_i \rightarrow T}, \dots, G_{S_M \rightarrow T}, D_A^i) \\ \left. + \mathcal{L}_{CCD}^{S_i}(G_{T \rightarrow S_1}, \dots, G_{T \rightarrow S_{i-1}}, G_{T \rightarrow S_{i+1}}, \dots, G_{T \rightarrow S_M}, G_{S_i \rightarrow T}, D_i) \right] \\ + \mathcal{L}_{task}(F, X', Y) + \mathcal{L}_{feat}(F_f, D_{F_f}, X', X_T). \end{aligned} \quad (9)$$

The training process corresponds to solving for a target model F according to the optimization:

$$F^* = \arg \min_F \min_D \max_G \mathcal{L}_{MADAN}(G, D, F), \quad (10)$$

where G and D represent all the generators and discriminators in Eq. (9), respectively.

4 Experiments

In this section, we first introduce the experimental settings and then compare the segmentation results of the proposed MADAN and several state-of-the-art approaches both quantitatively and qualitatively, followed by some ablation studies.

Table 2: Comparison with the state-of-the-art DA methods for semantic segmentation from GTA and SYNTHIA to Cityscapes. The best class-wise IoU and mIoU trained on the source domains are emphasized in bold (similar below).

Standards	Method	road	sidewalk	building	wall	fence	pole	t-light	t-sign	vegetation	sky	person	rider	car	bus	m-bike	bicycle	mIoU
Source-only	GTA	54.1	19.6	47.4	3.3	5.2	3.3	0.5	3.0	69.2	43.0	31.3	0.1	59.3	8.3	0.2	0.0	21.7
	SYNTHIA	3.9	14.5	45.0	0.7	0.0	14.6	0.7	2.6	68.2	68.4	31.5	4.6	31.5	7.4	0.3	1.4	18.5
	GTA+SYNTHIA	44.0	19.0	60.1	11.1	13.7	10.1	5.0	4.7	74.7	65.3	40.8	2.3	43.0	15.9	1.3	1.4	25.8
GTA-only DA	FCN Wld [47]	70.4	32.4	62.1	14.9	5.4	10.9	14.2	2.7	79.2	64.6	44.1	4.2	70.4	7.3	3.5	0.0	27.1
	CDA [48]	74.8	22.0	71.7	6.0	11.9	8.4	16.3	11.1	75.7	66.5	38.0	9.3	55.2	18.9	16.8	14.6	28.9
	ROAD [50]	85.4	31.2	78.6	27.9	22.2	21.9	23.7	11.4	80.7	68.9	48.5	14.1	78.0	23.8	8.3	0.0	39.0
	AdaptSeg [71]	87.3	29.8	78.6	21.1	18.2	22.5	21.5	11.0	79.7	71.3	46.8	6.5	80.1	26.9	10.6	0.3	38.3
	CyCADA [32]	85.2	37.2	76.5	21.8	15.0	23.8	22.9	21.5	80.5	60.7	50.5	9.0	76.9	28.2	4.5	0.0	38.7
	DCAN [55]	82.3	26.7	77.4	23.7	20.5	20.4	30.3	15.9	80.9	69.5	52.6	11.1	79.6	21.2	17.0	6.7	39.8
SYNTHIA-only DA	FCN Wld [47]	11.5	19.6	30.8	4.4	0.0	20.3	0.1	11.7	42.3	68.7	51.2	3.8	54.0	3.2	0.2	0.6	20.2
	CDA [48]	65.2	26.1	74.9	0.1	0.5	10.7	3.7	3.0	76.1	70.6	47.1	8.2	43.2	20.7	0.7	13.1	29.0
	ROAD [50]	77.7	30.0	77.5	9.6	0.3	25.8	10.3	15.6	77.6	79.8	44.5	16.6	67.8	14.5	7.0	23.8	36.2
	CyCADA [32]	66.2	29.6	65.3	0.5	0.2	15.1	4.5	6.9	67.1	68.2	42.8	14.1	51.2	12.6	2.4	20.7	29.2
Source-combined DA	DCAN [55]	79.9	30.4	70.8	1.6	0.6	22.3	6.7	23.0	76.9	73.9	41.9	16.7	61.7	11.5	10.3	38.6	35.4
	CyCADA [32]	82.8	35.8	78.2	17.5	15.1	10.8	6.1	19.4	78.6	77.2	44.5	15.3	74.9	17.0	10.3	12.9	37.3
Multi-source DA	MDAN [69]	64.2	19.7	63.8	13.1	19.4	5.5	5.2	6.8	71.6	61.1	42.0	12.0	62.7	2.9	12.3	8.1	29.4
	MADAN (Ours)	86.2	37.7	79.1	20.1	17.8	15.5	14.5	21.4	78.5	73.4	49.7	16.8	77.8	28.3	17.7	27.5	41.4
Oracle-Train on Tgt	FCN [5]	96.4	74.5	87.1	35.3	37.8	36.4	46.9	60.1	89.0	89.8	65.6	35.9	76.9	64.1	40.5	65.1	62.6

Table 3: Comparison with the state-of-the-art DA methods for semantic segmentation from GTA and SYNTHIA to BDDS. The best class-wise IoU and mIoU are emphasized in bold.

Standards	Method	road	sidewalk	building	wall	fence	pole	t-light	t-sign	vegetation	sky	person	rider	car	bus	m-bike	bicycle	mIoU
Source-only	GTA	50.2	18.0	55.1	3.1	7.8	7.0	0.0	3.5	61.0	50.4	19.2	0.0	58.1	3.2	19.8	0.0	22.3
	SYNTHIA	7.0	6.0	50.5	0.0	0.0	15.1	0.2	2.4	60.3	85.6	16.5	0.5	36.7	3.3	0.0	3.5	17.1
	GTA+SYNTHIA	54.5	19.6	64.0	3.2	3.6	5.2	0.0	0.0	61.3	82.2	13.9	0.0	55.5	16.7	13.4	0.0	24.6
GTA-only DA	CyCADA [32]	77.9	26.8	68.8	13.0	19.7	13.5	18.2	22.3	64.2	84.2	39.0	22.6	72.0	11.5	15.9	2.0	35.7
SYNTHIA-only DA	CyCADA [32]	55	13.8	45.2	0.1	0.0	13.2	0.5	10.6	63.3	67.4	22.0	6.9	52.5	10.5	10.4	13.3	24.0
Source-combined DA	CyCADA [32]	61.5	27.6	72.1	6.5	2.8	15.7	10.8	18.1	78.3	73.8	44.9	16.3	41.5	21.1	21.8	25.9	33.7
Multi-source DA	MDAN [69]	35.9	15.8	56.9	5.8	16.3	9.5	8.6	6.2	59.1	80.1	24.5	9.9	53.8	11.8	2.9	1.6	25.0
	MADAN (Ours)	60.2	29.5	66.6	16.9	10.0	16.6	10.9	16.4	78.8	75.1	47.5	17.3	48.0	24.0	13.2	17.3	36.3
Oracle-Train on Tgt	FCN [5]	91.7	54.7	79.5	25.9	42.0	23.6	30.9	34.6	81.2	91.6	49.6	23.5	85.4	64.2	28.4	41.1	53.0

4.1 Experimental Settings

Datasets. In our adaptation experiments, we use synthetic GTA [18] and SYNTHIA [19] datasets as the source domains and real Cityscapes [15] and BDDS [72] datasets as the target domains.

Baselines. We compare MADAN with the following methods. **(1) Source-only**, *i.e.* train on the source domains and test on the target domain directly. We can view this as a lower bound of DA. **(2) Single-source DA**, perform multi-source DA via single-source DA, including FCNs Wld [47], CDA [48], ROAD [50], AdaptSeg [71], CyCADA [32], and DCAN [55]. **(3) Multi-source DA**, extend some single-source DA method to multi-source settings, including MDAN [69]. For comparison, we also report the results of an oracle setting, where the segmentation model is both trained and tested on the target domain. For the source-only and single-source DA standards, we employ two strategies: (1) single-source, *i.e.* performing adaptation on each single source; (2) source-combined, *i.e.* all source domains are combined into a traditional single source. For MDAN, we extend the original classification network for our segmentation task.

Evaluation Metric. Following [47, 48, 32, 56], we employ mean intersection-over-union (mIoU) to evaluate the segmentation results. In the experiments, we take the 16 intersection classes of GTA and SYNTHIA, compatible with Cityscapes and BDDS, for all mIoU evaluations.

Implementation Details. Although MADAN could be trained in an end-to-end manner, due to constrained hardware resources, we train it in three stages. First, we train two CycleGANs (9 residual blocks for generator and 4 convolution layers for discriminator) [39] without semantic consistency loss, and then train an FCN F on the adapted images with corresponding labels from the source domains. Second, after updating F_A with F trained above, we generate adapted images using CycleGAN with the proposed DSC loss in Eq. (4) and aggregate different adapted domains using SAD and CCD. Finally, we train an FCN on the newly adapted images in the aggregated domain with feature-level alignment. The above stages are trained iteratively.

We choose to use FCN [5] as our semantic segmentation network, and, as the VGG family of networks is commonly used in reporting DA results, we use VGG-16 [73] as the FCN backbone. The weights

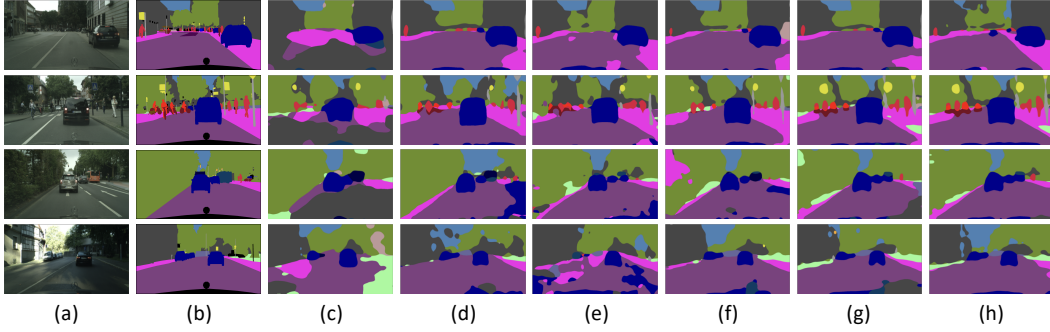


Figure 2: Qualitative semantic segmentation result from GTA and SYNTHIA to Cityscapes. From left to right are: (a) original image, (b) ground truth annotation, (c) source only from GTA, (d) CycleGANs on GTA and SYNTHIA, (e) +CCD+DSC, (f) +SAD+DSC, (g) +CCD+SAD+DSC, and (h) +CCD+SAD+DSC+Feat (MADAN).

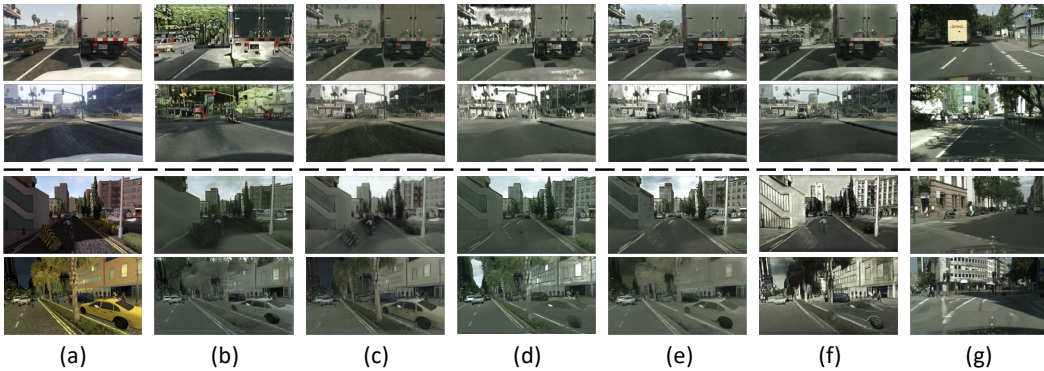


Figure 3: Visualization of image translation. From left to right are: (a) original source image, (b) CycleGAN, (c) CycleGAN+DSC, (d) CycleGAN+CCD+DSC, (e) CycleGAN+SAD+DSC, (f) CycleGAN+CCD+SAD+DSC, and (g) target Cityscapes image. The top two rows and bottom rows are $\text{GTA} \rightarrow \text{Cityscapes}$ and $\text{SYNTHIA} \rightarrow \text{Cityscapes}$, respectively.

of the feature extraction layers in the networks are initialized from models trained on ImageNet [74]. The network is implemented in PyTorch and trained with Adam optimizer [75] using a batch size of 8 with initial learning rate $1e-4$. All the images are resized to 600×1080 , and are then cropped to 400×400 during the training of the pixel-level adaptation for 20 epochs. SAD and CCD are frozen in the first 5 and 10 epochs, respectively.

4.2 Comparison with State-of-the-art

The performance comparisons between the proposed MADAN model and the other baselines, including source-only, single-source DA, and multi-source DA, as measured by class-wise IoU and mIoU are shown in Table 2 and Table 3. From the results, we have the following observations:

(1) The source-only method that directly transfers the segmentation models trained on the source domains to the target domain obtains the worst performance in most adaptation settings. This is obvious, because the joint probability distributions of observed images and labels are significantly different among the sources and the target, due to the presence of domain shift. Without domain adaptation, the direct transfer cannot well handle this domain gap. Simply combining different source domains performs better than each single source, which indicates the superiority of multiple sources over single source despite the domain shift among different sources.

(2) Comparing source-only with single-source DA respectively on GTA and SYNTHIA, it is clear that all adaptation methods perform better, which demonstrates the effectiveness of domain adaptation in semantic segmentation. Comparing the results of CyCADA in single-source and source-combined

Table 4: Comparison between the proposed dynamic semantic consistency (DSC) loss in MADAN and the original SC loss in [32] on Cityscapes. The better mIoU for each pair is emphasized in bold.

Source	Method	road	sidewalk	building	wall	fence	pole	t-light	t-sign	vegetation	sky	person	rider	car	bus	m-bike	bicycle	mIoU
GTA	CycleGAN+SC	85.6	30.7	74.7	14.4	13.0	17.6	13.7	5.8	74.6	69.9	38.2	3.5	72.3	5.0	3.6	0.0	32.7
	CycleGAN+DSC	76.6	26.0	76.3	17.3	18.8	13.6	13.2	17.9	78.8	63.9	47.4	14.8	72.2	24.1	19.8	10.8	38.1
	CyCADA w/ SC	85.2	37.2	76.5	21.8	15.0	23.8	21.5	22.9	80.5	60.7	50.5	9.0	76.9	28.2	9.8	0.0	38.7
	CyCADA w/ DSC	84.1	27.3	78.3	21.6	18.0	13.8	14.1	16.7	78.1	66.9	47.8	15.4	78.7	23.4	22.3	14.4	40.0
SYNTHIA	CycleGAN+SC	64.0	29.4	61.7	0.3	0.1	15.3	3.4	5.0	63.4	68.4	39.4	11.5	46.6	10.4	2.0	16.4	27.3
	CycleGAN + DSC	68.4	29.0	65.2	0.6	0.0	15.0	0.1	4.0	75.1	70.6	45.0	11.0	54.9	18.2	3.9	26.7	30.5
	CyCADA w/ SC	66.2	29.6	65.3	0.5	0.2	15.1	4.5	6.9	67.1	68.2	42.8	14.1	51.2	12.6	2.4	20.7	29.2
	CyCADA w/ DSC	69.8	27.2	68.5	5.8	0.0	11.6	0.0	2.8	75.7	58.3	44.3	10.5	68.1	22.1	11.8	32.7	31.8

Table 5: Comparison between the proposed dynamic semantic consistency (DSC) loss in MADAN and the original SC loss in [32] on BDDS. The better mIoU for each pair is emphasized in bold.

Source	Method	road	sidewalk	building	wall	fence	pole	t-light	t-sign	vegetation	sky	person	rider	car	bus	m-bike	bicycle	mIoU
GTA	CycleGAN+SC	62.1	20.9	59.2	6.0	23.5	12.8	9.2	22.4	65.9	78.4	34.7	11.4	64.4	14.2	10.9	1.9	31.1
	CycleGAN+DSC	74.4	23.7	65.0	8.6	17.2	10.7	14.2	19.7	59.0	82.8	36.3	19.6	69.7	4.3	17.6	4.2	32.9
	CyCADA w/ SC	68.8	23.7	67.0	7.5	16.2	9.4	11.3	22.2	60.5	82.1	36.1	20.6	63.2	15.2	16.6	3.4	32.0
	CyCADA w/ DSC	70.5	32.4	68.2	10.5	17.3	18.4	16.6	21.8	65.6	82.2	38.1	16.1	73.3	20.8	12.6	3.7	35.5
SYNTHIA	CycleGAN+SC	50.6	13.6	50.5	0.2	0.0	7.9	0.0	0.0	63.8	58.3	21.6	7.8	50.2	1.8	2.2	19.9	21.8
	CycleGAN + DSC	57.3	13.4	56.1	2.7	14.1	9.8	7.7	17.1	65.5	53.1	11.4	1.4	51.4	13.9	3.9	8.7	22.5
	CyCADA w/ SC	49.5	11.1	46.6	0.7	0.0	10.0	0.4	7.0	61.0	74.6	17.5	7.2	50.9	5.8	13.1	4.3	23.4
	CyCADA w/ DSC	55	13.8	45.2	0.1	0.0	13.2	0.5	10.6	63.3	67.4	22.0	6.9	52.5	10.5	10.4	13.3	24.0

settings, we can conclude that simply combining different source domains and performing single-source DA may result in performance degradation.

(3) MADAN achieves the highest mIoU score among all adaptation methods, and benefits from the joint consideration of pixel-level and feature-level alignments, cycle-consistency, dynamic semantic-consistency, domain aggregation, and multiple sources. MADAN also significantly outperforms source-combined DA, in which domain shift also exists among different sources. By bridging this gap, multi-source DA can boost the adaptation performance. On the one hand, compared to single-source DA [47, 48, 50, 71, 32, 55], MADAN utilizes more useful information from multiple sources. On the other hand, other multi-source DA methods [68, 69, 70] only consider feature-level alignment, which may be enough for coarse-grained tasks, *e.g.* image classification, but is obviously insufficient for fine-grained tasks, *e.g.* semantic segmentation, a pixel-wise prediction task. In addition, we consider pixel-level alignment with a dynamic semantic consistency loss and further aggregate different adapted domains.

(4) The oracle method that is trained on the target domain performs significantly better than the others. However, to train this model, the ground truth segmentation labels from the target domain are required, which are actually unavailable in UDA settings. We can deem this performance as a upper bound of UDA. Obviously, a large performance gap still exists between all adaptation algorithms and the oracle method, requiring further efforts on DA.

Visualization. The qualitative semantic segmentation results are shown in Figure 2. We can clearly see that after adaptation by the proposed method, the visual segmentation results are improved notably. We also visualize the results of pixel-level alignment from GTA and SYNTHIA to Cityscapes in Figure 3. We can see that with our final proposed pixel-level alignment method (f), the styles of the images are close to Cityscapes while the semantic information is well preserved.

4.3 Ablation Study

First, we compare the proposed dynamic semantic consistency (DSC) loss in MADAN with the original semantic consistency (SC) loss in CyCADA [32]. As shown in Table 4 and Table 5, we can see that for all simulation to real adaptations, DSC achieves better results. After demonstrating its value, we employ the DSC loss in subsequent experiments.

Second, we incrementally investigate the effectiveness of different components in MADAN on both Cityscapes and BDDS. The results are shown in Table 6 and Table 7. We can observe that: (1) both domain aggregation methods, *i.e.* SAD and CCD, can obtain better performance by making different adapted domains more closely aggregated, while SAD outperforms CCD; (2) adding the

Table 6: Ablation study on different components in MADAN on Cityscapes. Baseline denotes using pixel-level alignment with cycle-consistency, +SAD denotes using the sub-domain aggregation discriminator, +CCD denotes using the cross-domain cycle discriminator, +DSC denotes using the dynamic semantic consistency loss, and +Feat denotes using feature-level alignment.

Method	road	sidewalk	building	wall	fence	pole	t-light	t-sign	vegetation	sky	person	rider	car	bus	m-bike	bicycle	mIoU
Baseline	74.9	27.6	67.5	9.1	10.0	12.8	1.4	13.6	63.0	47.1	41.7	13.5	60.8	22.4	6.0	8.1	30.0
+SAD	79.7	33.2	75.9	11.8	3.6	15.9	8.6	15.0	74.7	78.9	44.2	17.1	68.2	24.9	16.7	14.0	36.4
+CCD	82.1	36.3	69.8	9.5	4.9	11.8	12.5	15.3	61.3	54.1	49.7	10.0	70.7	9.7	19.7	12.4	33.1
+SAD+CCD	82.7	35.3	76.5	15.4	19.4	14.1	7.2	13.9	75.3	74.2	50.9	19.0	66.5	26.6	16.3	6.7	37.5
+SAD+DSC	83.1	36.6	78.0	23.3	12.6	11.8	3.5	11.3	75.5	74.8	42.2	17.9	72.2	27.2	13.8	10.0	37.1
+CCD+DSC	86.8	36.9	78.6	16.2	8.1	17.7	8.9	13.7	75.0	74.8	42.2	18.2	74.6	22.5	22.9	12.7	38.1
+SAD+CCD+DSC	84.2	35.1	78.7	17.1	18.7	15.4	15.7	24.1	77.9	72.0	49.2	17.1	75.2	24.1	18.9	19.2	40.2
+SAD+CCD+DSC+Feat	86.2	37.7	79.1	20.1	17.8	15.5	14.5	21.4	78.5	73.4	49.7	16.8	77.8	28.3	17.7	27.5	41.4

Table 7: Ablation study on different components in MADAN on BDDS.

Method	road	sidewalk	building	wall	fence	pole	t-light	t-sign	vegetation	sky	person	rider	car	bus	m-bike	bicycle	mIoU
Baseline	31.3	17.4	55.4	2.6	12.9	12.4	6.5	18.0	63.2	79.9	21.2	5.6	44.1	14.2	6.1	11.7	24.6
+SAD	58.9	18.7	61.8	6.4	10.7	17.1	20.3	17.0	67.3	83.7	21.1	6.7	66.6	22.7	4.5	14.9	31.2
+CCD	52.7	13.6	63.0	6.6	11.2	17.8	21.5	18.9	67.4	84.0	9.2	2.2	63.0	21.6	2.0	14.0	29.3
+SAD+CCD	61.6	20.2	61.7	7.2	12.1	18.5	19.8	16.7	64.2	83.2	25.9	7.3	66.8	22.2	5.3	14.9	31.8
+SAD+DSC	60.2	29.5	66.6	16.9	10.0	16.6	10.9	16.4	78.8	75.1	47.5	17.3	48.0	24.0	13.2	17.3	34.3
+CCD+DSC	61.5	27.6	72.1	6.5	12.8	15.7	10.8	18.1	78.3	73.8	44.9	16.3	41.5	21.1	21.8	15.9	33.7
+SAD+CCD+DSC	64.6	38.0	75.8	17.8	13.0	9.8	5.9	4.6	74.8	76.9	41.8	24.0	69.0	20.4	23.7	11.3	35.3
+SAD+CCD+DSC+Feat	69.1	36.3	77.9	21.5	17.4	13.8	4.1	16.2	76.5	76.2	42.2	16.4	56.3	22.4	24.5	13.5	36.3

DSC loss could further improve the mIoU score, again demonstrating the effectiveness of DSC; (3) feature-level alignments also contribute to the adaptation task; (4) the modules are orthogonal to each other to some extent, since adding each one of them does not introduce performance degradation.

4.4 Discussions

Computation cost. Since the proposed framework deals with a harder problem, *i.e.* multi-source domain adaptation, more modules are used to align different sources, which results in a larger model. In our experiments, MADAN is trained on 4 NVIDIA Tesla P40 GPUs for 40 hours using two source domains which is about twice the training time as on a single source. However, MADAN does not introduce any additional computation during inference, which is the biggest concern in real industrial applications, *e.g.* autonomous driving.

On the poorly performing classes. There are two main reasons for the poor performance on certain classes (*e.g.* fence and pole): 1) lack of images containing these classes and 2) structural differences of objects between simulation images and real images (*e.g.* the trees in simulation images are much taller than those in real images). Generating more images for different classes and improving the diversity of objects in the simulation environment are two promising directions for us to explore in future work that may help with these problems.

5 Conclusion

In this paper, we studied multi-source domain adaptation for semantic segmentation from synthetic data to real data. A novel framework, termed Multi-source Adversarial Domain Aggregation Network (MADAN), is designed with three components. For each source domain, we generated adapted images with a novel dynamic semantic consistency loss. Further we proposed a sub-domain aggregation discriminator and cross-domain cycle discriminator to better aggregate different adapted domains. Together with other techniques such as pixel- and feature-level alignments as well as cycle-consistency, MADAN achieves 15.6%, 1.6%, 4.1%, and 12.0% mIoU improvements compared with best source-only, best single-source DA, source-combined DA, and other multi-source DA, respectively on Cityscapes from GTA and SYNTHIA, and 11.7%, 0.6%, 2.6%, 11.3% on BDDS. For further studies, we plan to investigate multi-modal DA, such as using both image and LiDAR data, to better boost the adaptation performance. Improving the computational efficiency of MADAN, with techniques such as neural architecture search, is another direction worth investigating.

Acknowledgments

This work is supported by Berkeley DeepDrive and the National Natural Science Foundation of China (No. 61701273).

References

- [1] Andreas Geiger, Philip Lenz, and Raquel Urtasun. Are we ready for autonomous driving? the kitti vision benchmark suite. In *IEEE Conference on Computer Vision and Pattern Recognition*, pages 3354–3361, 2012.
- [2] Zhang-Wei Hong, Yu-Ming Chen, Hsuan-Kung Yang, Shih-Yang Su, Tzu-Yun Shann, Yi-Hsiang Chang, Brian Hsi-Lin Ho, Chih-Chieh Tu, Tsu-Ching Hsiao, Hsin-Wei Hsiao, et al. Virtual-to-real: learning to control in visual semantic segmentation. In *International Joint Conference on Artificial Intelligence*, pages 4912–4920, 2018.
- [3] Özgün Çiçek, Ahmed Abdulkadir, Soeren S Lienkamp, Thomas Brox, and Olaf Ronneberger. 3d u-net: learning dense volumetric segmentation from sparse annotation. In *International Conference on Medical Image Computing and Computer Assisted Intervention*, pages 424–432, 2016.
- [4] Shatha Jaradat. Deep cross-domain fashion recommendation. In *ACM Conference on Recommender Systems*, pages 407–410, 2017.
- [5] Jonathan Long, Evan Shelhamer, and Trevor Darrell. Fully convolutional networks for semantic segmentation. In *IEEE Conference on Computer Vision and Pattern Recognition*, pages 3431–3440, 2015.
- [6] Ziwei Liu, Xiao Xiao Li, Ping Luo, Chen-Change Loy, and Xiaoou Tang. Semantic image segmentation via deep parsing network. In *IEEE International Conference on Computer Vision*, pages 1377–1385, 2015.
- [7] Shuai Zheng, Sadeep Jayasumana, Bernardino Romera-Paredes, Vibhav Vineet, Zhizhong Su, Dalong Du, Chang Huang, and Philip HS Torr. Conditional random fields as recurrent neural networks. In *IEEE International Conference on Computer Vision*, pages 1529–1537, 2015.
- [8] Guosheng Lin, Chunhua Shen, Anton Van Den Hengel, and Ian Reid. Efficient piecewise training of deep structured models for semantic segmentation. In *IEEE Conference on Computer Vision and Pattern Recognition*, pages 3194–3203, 2016.
- [9] Fisher Yu and Vladlen Koltun. Multi-scale context aggregation by dilated convolutions. In *International Conference on Learning Representations*, 2016.
- [10] Vijay Badrinarayanan, Alex Kendall, and Roberto Cipolla. Segnet: A deep convolutional encoder-decoder architecture for image segmentation. *IEEE Transactions on Pattern Analysis and Machine Intelligence*, 39(12):2481–2495, 2017.
- [11] Hengshuang Zhao, Jianping Shi, Xiaojuan Qi, Xiaogang Wang, and Jiaya Jia. Pyramid scene parsing network. In *IEEE Conference on Computer Vision and Pattern Recognition*, pages 2881–2890, 2017.
- [12] Liang-Chieh Chen, George Papandreou, Iasonas Kokkinos, Kevin Murphy, and Alan L Yuille. Deeplab: Semantic image segmentation with deep convolutional nets, atrous convolution, and fully connected crfs. *IEEE Transactions on Pattern Analysis and Machine Intelligence*, 40(4):834–848, 2017.
- [13] Panqu Wang, Pengfei Chen, Ye Yuan, Ding Liu, Zehua Huang, Xiaodi Hou, and Garrison Cottrell. Understanding convolution for semantic segmentation. In *IEEE Winter Conference on Applications of Computer Vision*, pages 1451–1460, 2018.
- [14] Bolei Zhou, Hang Zhao, Xavier Puig, Tete Xiao, Sanja Fidler, Adela Barriuso, and Antonio Torralba. Semantic understanding of scenes through the ade20k dataset. *International Journal of Computer Vision*, 127(3):302–321, 2019.
- [15] Marius Cordts, Mohamed Omran, Sebastian Ramos, Timo Rehfeld, Markus Enzweiler, Rodrigo Benenson, Uwe Franke, Stefan Roth, and Bernt Schiele. The cityscapes dataset for semantic urban scene understanding. In *IEEE Conference on Computer Vision and Pattern Recognition*, pages 3213–3223, 2016.

- [16] Antonio Torralba and Alexei A Efros. Unbiased look at dataset bias. In *IEEE Conference on Computer Vision and Pattern Recognition*, pages 1521–1528, 2011.
- [17] Bichen Wu, Xuanyu Zhou, Sicheng Zhao, Xiangyu Yue, and Kurt Keutzer. Squeezesegv2: Improved model structure and unsupervised domain adaptation for road-object segmentation from a lidar point cloud. In *IEEE International Conference on Robotics and Automation*, pages 4376–4382, 2019.
- [18] Stephan R Richter, Vibhav Vineet, Stefan Roth, and Vladlen Koltun. Playing for data: Ground truth from computer games. In *European Conference on Computer Vision*, pages 102–118, 2016.
- [19] German Ros, Laura Sellart, Joanna Materzynska, David Vazquez, and Antonio M Lopez. The synthia dataset: A large collection of synthetic images for semantic segmentation of urban scenes. In *IEEE Conference on Computer Vision and Pattern Recognition*, pages 3234–3243, 2016.
- [20] Xiangyu Yue, Bichen Wu, Sanjit A Seshia, Kurt Keutzer, and Alberto L Sangiovanni-Vincentelli. A lidar point cloud generator: from a virtual world to autonomous driving. In *ACM International Conference on Multimedia Retrieval*, pages 458–464, 2018.
- [21] Vishal M Patel, Raghuraman Gopalan, Ruonan Li, and Rama Chellappa. Visual domain adaptation: A survey of recent advances. *IEEE Signal Processing Magazine*, 32(3):53–69, 2015.
- [22] Shai Ben-David, John Blitzer, Koby Crammer, Alex Kulesza, Fernando Pereira, and Jennifer Wortman Vaughan. A theory of learning from different domains. *Machine learning*, 79(1-2):151–175, 2010.
- [23] Raghuraman Gopalan, Ruonan Li, and Rama Chellappa. Unsupervised adaptation across domain shifts by generating intermediate data representations. *IEEE Transactions on Pattern Analysis and Machine Intelligence*, 36(11):2288–2302, 2014.
- [24] Christos Louizos, Kevin Swersky, Yujia Li, Max Welling, and Richard Zemel. The variational fair autoencoder. *arXiv:1511.00830*, 2015.
- [25] Eric Tzeng, Judy Hoffman, Kate Saenko, and Trevor Darrell. Adversarial discriminative domain adaptation. In *IEEE Conference on Computer Vision and Pattern Recognition*, pages 2962–2971, 2017.
- [26] Sinno Jialin Pan and Qiang Yang. A survey on transfer learning. *IEEE Transactions on Knowledge and Data Engineering*, 22(10):1345–1359, 2010.
- [27] Xavier Glorot, Antoine Bordes, and Yoshua Bengio. Domain adaptation for large-scale sentiment classification: A deep learning approach. In *International Conference on Machine Learning*, pages 513–520, 2011.
- [28] I-Hong Jhuo, Dong Liu, DT Lee, and Shih-Fu Chang. Robust visual domain adaptation with low-rank reconstruction. In *IEEE Conference on Computer Vision and Pattern Recognition*, pages 2168–2175, 2012.
- [29] Carlos J Becker, Christos M Christoudias, and Pascal Fua. Non-linear domain adaptation with boosting. In *Advances in Neural Information Processing Systems*, pages 485–493, 2013.
- [30] Muhammad Ghifary, W Bastiaan Kleijn, Mengjie Zhang, and David Balduzzi. Domain generalization for object recognition with multi-task autoencoders. In *IEEE International Conference on Computer Vision*, pages 2551–2559, 2015.
- [31] Mingsheng Long, Yue Cao, Jianmin Wang, and Michael Jordan. Learning transferable features with deep adaptation networks. In *International Conference on Machine Learning*, pages 97–105, 2015.
- [32] Judy Hoffman, Eric Tzeng, Taesung Park, Jun-Yan Zhu, Phillip Isola, Kate Saenko, Alexei A Efros, and Trevor Darrell. Cycada: Cycle-consistent adversarial domain adaptation. In *International Conference on Machine Learning*, pages 1994–2003, 2018.
- [33] Baochen Sun, Jiashi Feng, and Kate Saenko. Return of frustratingly easy domain adaptation. In *AAAI Conference on Artificial Intelligence*, pages 2058–2065, 2016.
- [34] Baochen Sun, Jiashi Feng, and Kate Saenko. Correlation alignment for unsupervised domain adaptation. In *Domain Adaptation in Computer Vision Applications*, pages 153–171. 2017.

- [35] Junbao Zhuo, Shuhui Wang, Weigang Zhang, and Qingming Huang. Deep unsupervised convolutional domain adaptation. In *ACM International Conference on Multimedia*, pages 261–269, 2017.
- [36] Ian Goodfellow, Jean Pouget-Abadie, Mehdi Mirza, Bing Xu, David Warde-Farley, Sherjil Ozair, Aaron Courville, and Yoshua Bengio. Generative adversarial nets. In *Advances in Neural Information Processing Systems*, pages 2672–2680, 2014.
- [37] Konstantinos Bousmalis, Nathan Silberman, David Dohan, Dumitru Erhan, and Dilip Krishnan. Unsupervised pixel-level domain adaptation with generative adversarial networks. In *IEEE Conference on Computer Vision and Pattern Recognition*, pages 3722–3731, 2017.
- [38] Ming-Yu Liu and Oncel Tuzel. Coupled generative adversarial networks. In *Advances in Neural Information Processing Systems*, pages 469–477, 2016.
- [39] Jun-Yan Zhu, Taesung Park, Phillip Isola, and Alexei A Efros. Unpaired image-to-image translation using cycle-consistent adversarial networks. In *IEEE International Conference on Computer Vision*, pages 2223–2232, 2017.
- [40] Sicheng Zhao, Xin Zhao, Guiguang Ding, and Kurt Keutzer. Emotiongan: unsupervised domain adaptation for learning discrete probability distributions of image emotions. In *ACM International Conference on Multimedia*, pages 1319–1327, 2018.
- [41] Paolo Russo, Fabio M Carlucci, Tatiana Tommasi, and Barbara Caputo. From source to target and back: symmetric bi-directional adaptive gan. In *IEEE Conference on Computer Vision and Pattern Recognition*, pages 8099–8108, 2018.
- [42] Swami Sankaranarayanan, Yogesh Balaji, Carlos D Castillo, and Rama Chellappa. Generate to adapt: Aligning domains using generative adversarial networks. In *IEEE Conference on Computer Vision and Pattern Recognition*, pages 8503–8512, 2018.
- [43] Lanqing Hu, Meina Kan, Shiguang Shan, and Xilin Chen. Duplex generative adversarial network for unsupervised domain adaptation. In *IEEE Conference on Computer Vision and Pattern Recognition*, pages 1498–1507, 2018.
- [44] Sicheng Zhao, Chuang Lin, Pengfei Xu, Sendong Zhao, Yuchen Guo, Ravi Krishna, Guiguang Ding, and Kurt Keutzer. Cycleemotiongan: Emotional semantic consistency preserved cyclegan for adapting image emotions. In *AAAI Conference on Artificial Intelligence*, pages 2620–2627, 2019.
- [45] Muhammad Ghifary, W Bastiaan Kleijn, Mengjie Zhang, David Balduzzi, and Wen Li. Deep reconstruction-classification networks for unsupervised domain adaptation. In *European Conference on Computer Vision*, pages 597–613, 2016.
- [46] Konstantinos Bousmalis, George Trigeorgis, Nathan Silberman, Dilip Krishnan, and Dumitru Erhan. Domain separation networks. In *Advances in Neural Information Processing Systems*, pages 343–351, 2016.
- [47] Judy Hoffman, Dequan Wang, Fisher Yu, and Trevor Darrell. Fcns in the wild: Pixel-level adversarial and constraint-based adaptation. *arXiv:1612.02649*, 2016.
- [48] Yang Zhang, Philip David, and Boqing Gong. Curriculum domain adaptation for semantic segmentation of urban scenes. In *IEEE International Conference on Computer Vision*, pages 2020–2030, 2017.
- [49] Xingchao Peng, Ben Usman, Neela Kaushik, Judy Hoffman, Dequan Wang, and Kate Saenko. Visda: The visual domain adaptation challenge. *arXiv:1710.06924*, 2017.
- [50] Yuhua Chen, Wen Li, and Luc Van Gool. Road: Reality oriented adaptation for semantic segmentation of urban scenes. In *IEEE Conference on Computer Vision and Pattern Recognition*, pages 7892–7901, 2018.
- [51] Swami Sankaranarayanan, Yogesh Balaji, Arpit Jain, Ser Nam Lim, and Rama Chellappa. Learning from synthetic data: Addressing domain shift for semantic segmentation. In *IEEE Conference on Computer Vision and Pattern Recognition*, pages 3752–3761, 2018.
- [52] Yiheng Zhang, Zhaofan Qiu, Ting Yao, Dong Liu, and Tao Mei. Fully convolutional adaptation networks for semantic segmentation. In *IEEE Conference on Computer Vision and Pattern Recognition*, pages 6810–6818, 2018.

- [53] Aysegul Dundar, Ming-Yu Liu, Ting-Chun Wang, John Zedlewski, and Jan Kautz. Domain stylization: A strong, simple baseline for synthetic to real image domain adaptation. *arXiv:1807.09384*, 2018.
- [54] Xinge Zhu, Hui Zhou, Ceyuan Yang, Jianping Shi, and Dahua Lin. Penalizing top performers: Conservative loss for semantic segmentation adaptation. In *European Conference on Computer Vision*, pages 568–583, 2018.
- [55] Zuxuan Wu, Xintong Han, Yen-Liang Lin, Mustafa Gokhan Uzunbas, Tom Goldstein, Ser Nam Lim, and Larry S Davis. Dcan: Dual channel-wise alignment networks for unsupervised scene adaptation. In *European Conference on Computer Vision*, pages 518–534, 2018.
- [56] Xiangyu Yue, Yang Zhang, Sicheng Zhao, Alberto Sangiovanni-Vincentelli, Kurt Keutzer, and Boqing Gong. Domain randomization and pyramid consistency: Simulation-to-real generalization without accessing target domain data. In *IEEE International Conference on Computer Vision*, 2019.
- [57] Matthew Riemer, Ignacio Cases, Robert Ajemian, Miao Liu, Irina Rish, Yuhai Tu, and Gerald Tesaro. Learning to learn without forgetting by maximizing transfer and minimizing interference. In *International Conference on Learning Representations*, 2019.
- [58] Shiliang Sun, Honglei Shi, and Yuanbin Wu. A survey of multi-source domain adaptation. *Information Fusion*, 24:84–92, 2015.
- [59] Lixin Duan, Ivor W Tsang, Dong Xu, and Tat-Seng Chua. Domain adaptation from multiple sources via auxiliary classifiers. In *International Conference on Machine Learning*, pages 289–296, 2009.
- [60] Qian Sun, Rita Chattopadhyay, Sethuraman Panchanathan, and Jieping Ye. A two-stage weighting framework for multi-source domain adaptation. In *Advances in Neural Information Processing Systems*, pages 505–513, 2011.
- [61] Lixin Duan, Dong Xu, and Shih-Fu Chang. Exploiting web images for event recognition in consumer videos: A multiple source domain adaptation approach. In *IEEE Conference on Computer Vision and Pattern Recognition*, pages 1338–1345, 2012.
- [62] Rita Chattopadhyay, Qian Sun, Wei Fan, Ian Davidson, Sethuraman Panchanathan, and Jieping Ye. Multisource domain adaptation and its application to early detection of fatigue. *ACM Transactions on Knowledge Discovery from Data*, 6(4):18, 2012.
- [63] Lixin Duan, Dong Xu, and Ivor Wai-Hung Tsang. Domain adaptation from multiple sources: A domain-dependent regularization approach. *IEEE Transactions on Neural Networks and Learning Systems*, 23(3):504–518, 2012.
- [64] Jun Yang, Rong Yan, and Alexander G Hauptmann. Cross-domain video concept detection using adaptive svms. In *ACM International Conference on Multimedia*, pages 188–197, 2007.
- [65] Gabriele Schweikert, Gunnar Rätsch, Christian Widmer, and Bernhard Schölkopf. An empirical analysis of domain adaptation algorithms for genomic sequence analysis. In *Advances in Neural Information Processing Systems*, pages 1433–1440, 2009.
- [66] Zhijie Xu and Shiliang Sun. Multi-source transfer learning with multi-view adaboost. In *International Conference on Neural information processing*, pages 332–339, 2012.
- [67] Shi-Liang Sun and Hong-Lei Shi. Bayesian multi-source domain adaptation. In *International Conference on Machine Learning and Cybernetics*, volume 1, pages 24–28, 2013.
- [68] Ruijia Xu, Ziliang Chen, Wangmeng Zuo, Junjie Yan, and Liang Lin. Deep cocktail network: Multi-source unsupervised domain adaptation with category shift. In *IEEE Conference on Computer Vision and Pattern Recognition*, pages 3964–3973, 2018.
- [69] Han Zhao, Shanghang Zhang, Guanhang Wu, José MF Moura, Joao P Costeira, and Geoffrey J Gordon. Adversarial multiple source domain adaptation. In *Advances in Neural Information Processing Systems*, pages 8568–8579, 2018.
- [70] Xingchao Peng, Qinxun Bai, Xide Xia, Zijun Huang, Kate Saenko, and Bo Wang. Moment matching for multi-source domain adaptation. *arXiv:1812.01754*, 2018.
- [71] Yi-Hsuan Tsai, Wei-Chih Hung, Samuel Schuster, Kihyuk Sohn, Ming-Hsuan Yang, and Manmohan Chandraker. Learning to adapt structured output space for semantic segmentation. In *IEEE Conference on Computer Vision and Pattern Recognition*, pages 7472–7481, 2018.

- [72] Fisher Yu, Wenqi Xian, Yingying Chen, Fangchen Liu, Mike Liao, Vashisht Madhavan, and Trevor Darrell. Bdd100k: A diverse driving video database with scalable annotation tooling. *arXiv:1805.04687*, 2018.
- [73] Karen Simonyan and Andrew Zisserman. Very deep convolutional networks for large-scale image recognition. In *International Conference on Learning Representations*, 2015.
- [74] Jia Deng, Wei Dong, Richard Socher, Li-Jia Li, Kai Li, and Li Fei-Fei. Imagenet: A large-scale hierarchical image database. In *IEEE Conference on Computer Vision and Pattern Recognition*, pages 248–255, 2009.
- [75] Diederik P Kingma and Jimmy Ba. Adam: A method for stochastic optimization. In *International Conference on Learning Representations*, 2015.